

Magnetic Skyrmions: from lumps to supercompactons

Stefano Bolognesi^(1,*), Sven Bjarke Gudnason^(2,†), Roberto Menta^(3,‡)

⁽¹⁾*Department of Physics “E. Fermi”, University of Pisa, and INFN, Sezione di Pisa
Largo Pontecorvo, 3, Ed. C, 56127 Pisa, Italy*

⁽²⁾*Institute of Contemporary Mathematics, School of Mathematics and Statistics,
Henan University, Kaifeng, Henan 475004, P. R. China*

⁽³⁾*Scuola Normale Superiore, Piazza dei Cavalieri, 7, and Laboratorio NEST,
Piazza S. Silvestro, 12, 56127 Pisa, Italy*

^(*)stefano.bolognesi@unipi.it, ^(†)gudnason@henu.edu.cn, ^(‡)roberto.menta@sns.it

Abstract

The magnetic Skyrmion is described by one control parameter and one length scale. We study the two extreme limits of the control parameter – infinitely large and vanishing – and find that the magnetic Skyrmion becomes a “restricted” magnetic Skyrmion and an $O(3)$ sigma model lump, respectively. Depending on the potential under consideration, the restricted limit manifests differently. In the case of the Zeeman term, the restricted magnetic Skyrmion becomes a “supercompacton” that develops a discontinuity, whereas for the Zeeman term to the power $3/2$ it becomes a normal compacton. In both the lump and the restricted limit the solution is given in exact explicit form. We observe that the case of the Zeeman term squared, which can also be understood as a special combination of the Zeeman term and the easy-plane potential – realizable in the laboratory, the analytically exact solution for all values of the coupling – including the BPS case – is also of the lump type. Finally, we notice that certain materials (e.g. $\text{Fe}_{1-x}\text{Co}_x\text{Si}$ or $\text{Mn}_{1-x}\text{Fe}_x\text{Ge}$) have a rather large control parameter ϵ of order 100, making the restricted limit a suitable rough approximation.

Contents

1	Introduction	2
2	2D Magnetic Skyrmions	4
2.1	Hedgehog Solution	9
2.2	The DM term and integration-by-parts	11
2.3	O(3) sigma model limit	12
2.4	Restricted model limit	13
2.5	Critical coupling	15
2.6	Analytic solution at any coupling	16
2.7	Numerical solutions	17
2.8	Comparison with experiments	22
3	Conclusion	23
A	Continuum Limit	24

1 Introduction

Topological soliton applications cover many fields of theoretical physics, from high energy physics to condensed matter theory [1–6]. Some topological solitons that have garnered significant attention in the field of condensed matter physics in recent years are known as *magnetic Skyrmions* named after the famous works of T. Skyrme [7, 8]. These magnetic Skyrmions are the main focus of this work. From a condensed matter point of view, a magnetic Skyrmion is a stable two-dimensional nanoparticle describing a localized winding of the magnetization in certain magnetic materials [9–11]. These topological defects are subject of intense experimental and theoretical investigations [12–25] and have shown potential for technological spintronic applications [26, 27]. They were observed for the first time in 2009 by S. Muhlbauer *et al.* [28] in a chiral magnet of MnSi, and subsequently in a plethora of other chiral magnets [29–34]. Magnetic Skyrmions have risen to prominence as up-and-coming candidates for next-generation high-density efficient information encoding [35, 36] or for quantum computing applications [37].

The spin texture of a magnetic Skyrmion is a stable configuration that originates from chiral interactions, known as Dzyaloshinskii–Moriya (DM) interactions. The Hamiltonian interaction term involving two atomic spins in the chiral magnet, was proposed by Dzyaloshinskii [38] as an additional contribution to the usual Heisenberg Hamiltonian. Subsequently, Moriya [39, 40] demonstrated that this type of interaction originates from the

relativistic spin-orbit coupling. It was suggested [41] to consider the mean field approximation (MFT) for the field theory model in the continuum limit, where both the Heisenberg exchange term (also called Dirichlet term, E_2) and the DM one (E_1) are competing and the Zeeman energy (the external potential, E_0) is included to control the system.

In this work we consider the theory of magnetic Skyrmions in two spatial dimensions (2D) and apply certain techniques used in the past in the context of the baby-Skyrme model [42]. We show that a dimensionless parameter enables us to control the relation between the Dirichlet term, the one with two derivatives, and the rest of the energy functional that contains the potential and the DM term. By changing this parameter we can flow from an almost BPS theory, close to the $O(3)$ sigma model which admits lumps as solutions, to a “restricted” magnetic Skyrmion model with just E_1 and E_0 . The restricted model is analytically solvable. In the case of the ordinary Zeeman potential, which is quadratic in the perturbative excitation fields near the vacuum, a feature never encountered before in the context of the baby-Skyrme model is present: the solution is not only a compacton¹ but it is also discontinuous. We may call it a “supercompacton”. The discontinuity is resolved as soon as we turn on a small coefficient for the Dirichlet term. We also study another subtlety of the model; that is, the DM term can be integrated by parts without changing the equation of motion or the energy when the potential is the Zeeman term (giving rise to exponential falloff). However, it turns out that for potentials that give rise to massless perturbative excitations, e.g. the Zeeman squared term, which can be understood as a specific linear combination of the Zeeman term and the easy-plane potential, discarding a boundary term and using a different DM term in the energy functional, is crucial for computing the correct sizes of the solutions in the lump limit, i.e. the limit of the control parameter going to zero.

Finally, we observe that this lump-type solution corresponds to the solution of the critically coupled version of magnetic Skyrmions with the Zeeman term squared, as described by Barton-Singer *et al.* [19]. It is not limited to this scenario: it is also the solution to the full second-order variational equation of motion for *all* values of the coupling [19]. We find that for this potential, discarding the boundary term changes the energy functional to become dependent on ϵ , hence revealing a phase transition between the homogeneous phase and the Skyrmionic phase.

On the experimental side, we also confront the dimensionless parameter with the various experimental realizations of the magnetic Skyrmion and find that the (near) “restricted” magnetic Skyrmion – corresponding to the case of a large control parameter – is actually realized in some materials, like $\text{Fe}_{1-x}\text{Co}_x\text{Si}$ or $\text{Mn}_{1-x}\text{Fe}_x\text{Ge}$. We also confirm that it is

¹Compactons are solitonic solutions with compact support: they have a nontrivial profile function for $r < R$ and vanishing energy outside, i.e. for $r > R$. Often the fields are continuous but their derivatives are not at $r = R$. Compactons exist in the baby-Skyrme model [43–45], the BPS-Skyrme model [46], as Q-balls in the gauged (ungauged) CP^N model [47]([48]) and in K-field theories [49], etc.

possible to experimentally realize the Zeeman squared term, by using magnets with a certain anisotropy term and adjusting the magnetic field of the Zeeman term, so as to complete the square. At this critically tuned value of the magnetic field, the exact analytic lump-type solution is thus realizable in the laboratory.

This paper is organized as follows. In Sec. 2 we review the magnetic Skyrmion in the continuum formulation with various potentials in our notation. In Sec. 2.1, we review the hedgehog Ansatz and discuss the symmetry breaking properties leading to the fixing of the phase parameter. In Sec. 2.2, we discuss integration-by-parts identities that do not alter the equations of motion or the energy for the case of the Zeeman term. In Secs. 2.3 and 2.4 we introduce the sigma model lump and restricted limits of the magnetic Skyrmion. In Sec. 2.5 we review the case of the critical coupling and in Sec. 2.6 we show that the lump solution is a solution to the model with the Zeeman term squared for any coupling. In Sec. 2.7 we provide numerical solutions that interpolate between the lump and restricted limits, verifying the analytical results obtained. In Sec. 2.8 we compare the control parameter to experimental parameters of various chiral magnets. We conclude in Sec. 3 with a discussion.

2 2D Magnetic Skyrmions

A magnetic Skyrmion is a stable *vortex-like* configuration of magnetic spin vectors [9–11]. The relevant physical quantity in a 2-dimensional magnet is the direction of the magnetization vector, \mathbf{n} . The latter is the order parameter for the system of spins \mathbf{S}_i , localized on the sites of 2-dimensional lattices. The simplest model describing such a system is given by the Heisenberg Hamiltonian

$$\mathcal{H}_H = - \sum_{i < j}^N \mathbb{J}_{ij} \mathbf{S}_i \cdot \mathbf{S}_j, \quad (2.1)$$

where the interaction is only between nearest neighbor's spins, and \mathbb{J}_{ij} is the exchange interaction constant (which is negative in ferromagnetic systems). We suppose that $\mathbb{J}_{ij} = J$ for all $\{j = i + 1 \mid i, j \in [1, N]\}$ with N a large integer number. In the mean field approximation, a proper dynamical variable is the expectation value of the spins, i.e. the unit magnetization vector $\mathbf{n} \in S^2$. Its dynamics is governed by the continuum Ginzburg-Landau (GL) effective theory (see e.g. Ref. [6]). This is the static energy of the O(3) sigma model. Furthermore, the Hamiltonian of the Heisenberg model can be supplemented by the potential-like term $-\mathbf{B} \cdot \mathbf{n}$ that describes the Zeeman interaction with an external magnetic field, which we choose to be aligned along the third Cartesian axis, $\mathbf{B} = B\mathbf{e}_3$.

In cubic crystals, without an inversion center, such as MnSi, symmetry analysis reveals an additional term that can be incorporated into the GL description, known as the

Dzyaloshinskii-Moriya (DM) interaction [38–40]:

$$\mathcal{H}_{\text{DM}} = - \sum_{ij}^N \mathbf{D}_{ij} \cdot (\mathbf{S}_i \times \mathbf{S}_j) , \quad (2.2)$$

where \mathbf{D}_{ij} is the chiral coupling parameter (supposed to be equal to D for all $\{j = i + 1 \mid i, j \in [1, N]\}$) which depends on the material. The corresponding energy in the continuum limit (see App. A), at the leading order in the long-wavelength approximation, reduces to the functional:

$$\begin{aligned} E[\mathbf{n}] &= \int d^2x J \left(\frac{1}{2} \partial_i \mathbf{n} \cdot \partial_i \mathbf{n} + \kappa \epsilon_{iab} \partial^i n^a n^b + h(1 - n_3) \right) \\ &\equiv E_2 + E_1 + E_0 , \end{aligned} \quad (2.3)$$

where $\mathbf{n} = (n^1, n^2, n^3)$ is a unit magnetization vector ($\mathbf{n} \cdot \mathbf{n} = 1$), $i = 1, 2$ are planar indices, $a, b = 1, 2, 3$ are (target) spatial indices, $\kappa = \frac{2D}{J}$ is the effective DM coupling and $h = \frac{|B|}{J}$ is the parameter playing the role of the mass or Zeeman coupling strength. The DM term, E_1 , breaks parity but is invariant under a simultaneous O(3) rotation of spin and O(2) rotation of spatial coordinates, a property inherited from its origin as a spin-orbit interaction.

In presence of a generic potential term E_0 , the energy functional takes the form

$$E[\mathbf{n}] = \int d^2x \left(\frac{1}{2} \partial_i \mathbf{n} \cdot \partial_i \mathbf{n} + \kappa \epsilon_{iab} \partial^i n^a n^b + V_p(\mathbf{n}) + \frac{\lambda}{2} (\mathbf{n} \cdot \mathbf{n} - 1) \right) , \quad (2.4)$$

where we have introduced the Lagrange multiplier, λ , to enforce the unit-length constraint ($\mathbf{n} \cdot \mathbf{n} = 1$) and we simply measure the energy in units of J . We choose to work with the class of potentials $E_0 = \int V_p(\mathbf{n}) d^2x$, that are parametrized by

$$V_p(\mathbf{n}) = h (1 - \mathbf{n} \cdot \mathbf{N})^p , \quad (2.5)$$

which corresponds to the usual massive Zeeman term for $p = 1$. Note that $\mathbf{N} = N^a \mathbf{e}_a$ is the vacuum field. The perturbative fields have mass $m = \sqrt{h}$ if $p = 1$ and $m = 0$ if $p > 1$. We will concentrate on the cases $p = 1, \frac{3}{2}, 2$ in this paper. The case $p = 2$ corresponds to a particular linear combination of the Zeeman term and the so-called easy-plane term

$$h (1 - \mathbf{n} \cdot \mathbf{N})^2 = 2h(1 - \mathbf{n} \cdot \mathbf{N}) + h(\mathbf{n} \cdot \mathbf{N})^2 - h . \quad (2.6)$$

We will later be using the fact that the DM term can be integrated by parts

$$E[\mathbf{n}] = \int d^2x \left(\frac{1}{2} \partial_i \mathbf{n} \cdot \partial_i \mathbf{n} + \kappa \sum_{b=1}^2 \epsilon_{iab} \partial^i n^a n^b - \kappa \epsilon_{ia3} n^a \partial^i n^3 + V_p(\mathbf{n}) + \text{t.d.} \right) , \quad (2.7)$$

where the total derivative reads t.d. = $\kappa \partial_i (\epsilon_{ia3} n^a n^3)$.

We can write the DM term in an invariant form. For this we need a tensor T^{ai} such that the DM term can be written as

$$\mathcal{E}_1 = \kappa \epsilon_{abc} T^{ai} \partial_i n^b n^c . \quad (2.8)$$

The transformations are SO(3) for the internal indices a, b, c and SO(2) for the spatial index i . Any tensor related by SO(3) and SO(2) transformations to this is essentially equivalent. Those are the tensors that leave invariant the maximal amount of symmetry, SO(2)_{diag}. We can express the tensors of this form in an invariant way. The choice is essentially determined once we pair $i = 1, 2$ with two corresponding orthogonal unit vectors T^{ai} in \mathbb{R}^3 , i.e.,

$$T^{a1} T^{a1} = T^{a2} T^{a2} = 1 , \quad T^{a1} T^{a2} = 0 . \quad (2.9)$$

So the meaning of \mathbf{T} is a pair of orthogonal unit vectors in \mathbb{R}^3 . The functional (2.3) corresponds to the choice

$$\mathbf{T} = \begin{pmatrix} 1 & 0 \\ 0 & 1 \\ 0 & 0 \end{pmatrix} , \quad \mathbf{N} = \begin{pmatrix} 0 \\ 0 \\ 1 \end{pmatrix} . \quad (2.10)$$

The equations of motion are

$$\partial_i^2 n^a + hp N^a (1 - \mathbf{n} \cdot \mathbf{N})^{p-1} - 2\kappa \epsilon_{aib} \partial^i n^b - \lambda n^a = 0 , \quad \mathbf{n} \cdot \mathbf{n} = 1 , \quad (2.11)$$

where the Lagrange multiplier is

$$\lambda = n^a (\partial_i^2 n^a + hp N^a (1 - \mathbf{n} \cdot \mathbf{N})^{p-1} - 2\kappa \epsilon_{aib} \partial^i n^b) . \quad (2.12)$$

The vector $\mathbf{N} = \mathbf{e}_3 = (0, 0, 1)$ corresponds to the vacuum. Due to the following condition

$$\lim_{r \rightarrow \infty} \mathbf{n} = \mathbf{N} , \quad (2.13)$$

the base space of the vector field $\mathbf{n} : \mathbb{R}^2 \rightarrow S^2$, can be compactified to the sphere S^2 . Therefore, due to the nontrivial homotopy group $\pi_2(S^2) = \mathbb{Z}$, there are topologically nontrivial solutions (with finite energy) that can be classified according to the degree of the map $\mathbf{n} : S^2 \rightarrow S^2$, i.e. the winding number $Q \in \mathbb{Z}$. The topological degree or the Skyrmion number, Q , is given by

$$Q = \int d^2x \mathcal{Q} = \frac{1}{4\pi} \int d^2x \mathbf{n} \cdot \partial_1 \mathbf{n} \times \partial_2 \mathbf{n} . \quad (2.14)$$

The target space S^2 can be parameterized by the angles (ϑ, φ) :

$$\mathbf{n} = \begin{pmatrix} \sin \vartheta \cos \varphi \\ \sin \vartheta \sin \varphi \\ \cos \vartheta \end{pmatrix}, \quad \vartheta \in [0, \pi], \quad \varphi \in [0, 2\pi). \quad (2.15)$$

and the energy functional (2.7) becomes

$$E[\vartheta, \varphi] = \int d^2x \left(\frac{1}{2}(\partial_i \vartheta)^2 + \frac{1}{2} \sin^2 \vartheta (\partial_i \varphi)^2 + h(1 - \cos \vartheta)^p + 2\kappa \sin^2 \vartheta (\sin \varphi \partial_1 \vartheta - \cos \varphi \partial_2 \vartheta) + \text{t.d.} \right), \quad (2.16)$$

where t.d. is a total derivative

$$\text{t.d.} = \frac{\kappa}{2} [\partial_1(\sin(2\vartheta) \sin \varphi) - \partial_2(\sin(2\vartheta) \cos \varphi)]. \quad (2.17)$$

Derrick's argument allows for the existence of these 2D magnetic solitons. The idea is to make a rescaling of the field $\mathbf{n}(x) \mapsto \mathbf{n}(x/R)$, and see how the energy terms scale with R , i.e.,

$$E_{\mathbf{n}}(R) \equiv E[\mathbf{n}(x/R)] = E_{2,\mathbf{n}}(1) + E_{1,\mathbf{n}}(1)R + E_{0,\mathbf{n}}(1)R^2, \quad (2.18)$$

where the three terms correspond to the kinetic energy, the DM term and the potential term, respectively. If the DM term is negative, $E_{\mathbf{n}}(R)$ starts, for small R , decreasing linearly with R until it increases quadratically due to the potential contribution. This change allows for the existence of stationary points corresponding to

$$R_* = \frac{E_{1,\mathbf{n}}(1)}{2E_{0,\mathbf{n}}(1)}, \quad (2.19)$$

which is roughly the length scale at which a soliton can be stabilized. By using the order of magnitude estimate

$$E_{2,\mathbf{n}}(1) \propto 1, \quad E_{1,\mathbf{n}}(1) \propto \kappa, \quad E_{0,\mathbf{n}}(1) \propto h, \quad (2.20)$$

we have

$$R_* \sim \frac{\kappa}{h}. \quad (2.21)$$

The length scale of the soliton thus increases with κ and decreases with h . We thus define two new parameters:

$$\ell = \frac{\kappa}{h}, \quad \epsilon = \frac{\kappa^2}{h}, \quad (2.22)$$

where ℓ controls the size of the Skyrmion (2.19) while ϵ , the dimensionless parameter of the theory, controls the relation between E_2 and $E_1 + E_0$. In order to see the scaling behavior of the theory, we can write

$$E_{\mathbf{n}} = \tilde{E}_{2,\mathbf{n}} + \kappa \tilde{E}_{1,\mathbf{n}} + h \tilde{E}_{0,\mathbf{n}} , \quad (2.23)$$

and perform the scaling $\mathbf{n}(x) \mapsto \mathbf{n}(x/\ell)$, which yields

$$E_{\mathbf{n}} = \tilde{E}_{2,\mathbf{n}} + \epsilon \tilde{E}_{1,\mathbf{n}} + \epsilon \tilde{E}_{0,\mathbf{n}} . \quad (2.24)$$

Clearly, in the limit of small ϵ , there is only the kinetic term, whereas in the limit of large ϵ , there is only a small contribution from the kinetic term. In these rescaled coordinates, the soliton size is of order one. On the other hand, if we instead perform the following rescaling $\mathbf{n}(x) \mapsto \mathbf{n}(x\kappa)$, we obtain

$$E_{\mathbf{n}} = \tilde{E}_{2,\mathbf{n}} + \tilde{E}_{1,\mathbf{n}} + \frac{1}{\epsilon} \tilde{E}_{0,\mathbf{n}} . \quad (2.25)$$

In these rescaled coordinates, it is clear that the model only depends on ϵ , but now the size of the soliton is no longer of order one, but of order ϵ .

The symmetry group $\text{SO}(3)_{\text{int}}$ (internal) of the sigma model is broken to $\text{SO}(2)_{\text{int}}$ by the potential, viz. by the vector \mathbf{N} in E_0 . So, by considering $E_2 + E_0$, we have a symmetry group of spatial and internal rotations, $\text{SO}(2)_{\text{spt}} \times \text{SO}(2)_{\text{int}}$. The DM term locks together spatial and internal rotations, so only a diagonal combination of the two remains invariant, $\text{SO}(2)_{\text{diag}}$. Rotations of $\text{SO}(2)_{\text{diag}}$ act as:

$$\mathbf{n}(x_1, x_2) \mapsto R_{12}(\zeta) \mathbf{n}(\cos \zeta x_1 - \sin \zeta x_2, \sin \zeta x_1 + \cos \zeta x_2) , \quad \zeta \in [0, 2\pi) . \quad (2.26)$$

Moreover, there are the two internal parities as a discrete group $P_{\text{spt}} \times P_{\text{int}}$. The DM interaction is responsible for the breaking to the diagonal group P_{diag} . Up to an additional internal rotation of π , the parity transformations act as:

$$\mathbf{n}(x_1, x_2) \mapsto \bar{\mathbf{n}}(x_1, -x_2) , \quad \bar{\mathbf{n}} = (n^1, -n^2, n^3) . \quad (2.27)$$

Therefore, the total invariance group of the model is given by

$$G = P_{\text{diag}} \times \text{SO}(2)_{\text{diag}} \times T_2 , \quad (2.28)$$

where T_2 corresponds to the 2-dimensional translations.

We can now briefly consider the perturbative spectrum of the theory near the vacuum of the potential. In order to do so, we expand the fields as: $\mathbf{n} \rightarrow \mathbf{N} + \mathbf{u}$ and insert it into the static energy density (2.3) for the class of potentials (2.5):

$$\mathcal{E} \simeq \frac{1}{2} \partial_i \mathbf{u} \cdot \partial_i \mathbf{u} + V_p(\mathbf{u}) + \text{t.d.} , \quad (2.29)$$

where $i, j = 1, 2$, $E = \int \mathcal{E} d^2x$ and t.d. stands for total derivative. The Lagrangian density of the system is:

$$\mathcal{L}[\mathbf{u}] = \frac{1}{2} \partial_0 \mathbf{u} \cdot \partial_0 \mathbf{u} - \mathcal{E} , \quad (2.30)$$

where Lorentz invariance is explicitly broken by the DM term. At the quadratic level the DM term contributes only with a linear term which is also a total derivative, thus the spectrum of the perturbative particles is not changed from the O(3) sigma model with the potential V_p [50]. When \mathbf{T} and \mathbf{N} are not orthogonal there may be a quadratic contribution from the DM term.

2.1 Hedgehog Solution

The 2-dimensional base space can be parameterized by the polar coordinates (r, ϕ) where $r > 0$ and $\phi \in [0, 2\pi]$ as $x_1 + ix_2 = r e^{i\phi}$. We seek solutions within the class of hedgehog maps and can express the hedgehog Ansatz as

$$\vartheta = \vartheta(r) , \quad \varphi = -Q\phi + \delta , \quad (2.31)$$

where $\vartheta(r)$ is the profile function of the soliton. Since the field must approach the vacuum $\mathbf{N} = (0, 0, 1)$ at spatial infinity, it satisfies the boundary conditions: $\vartheta(0) = \pi$ and $\vartheta(\infty) = 0$. The phase δ corresponds to the internal orientation of the Skyrmion, i.e. a generic rotation in x_1 - x_2 plane. Substituting the Ansatz (2.31) into the energy functional (2.3) and integrating over φ , we find that

$$E = 2\pi \int r dr \left\{ \frac{1}{2} (\vartheta')^2 + \frac{Q^2}{2r^2} \sin^2 \vartheta + h(1 - \cos \vartheta)^p + \frac{\kappa}{\pi(Q+1)} \sin(Q\pi) \sin(\delta - Q\pi) \left(\vartheta' - \frac{Q}{2r} \sin(2\vartheta) \right) \right\} , \quad (2.32)$$

and the topological charge (2.14) reduces to

$$Q = -\frac{Q}{2} \int \sin(\vartheta) \vartheta' dr = -\frac{Q}{2} \int_{\pi}^0 \sin(\vartheta) d\vartheta = -\frac{Q}{2} [\cos \vartheta]_0^{\pi} = Q . \quad (2.33)$$

We note that the contribution of the DM interaction energy is nontrivial only for the rotationally invariant configuration with topological charge $Q = -1$. Indeed we have that

$$\frac{\kappa}{\pi(Q+1)} \sin(Q\pi) \sin(\delta - Q\pi) = \begin{cases} \kappa \sin \delta & \text{if } Q = -1 , \\ 0 & \text{if } Q \neq -1 . \end{cases} \quad (2.34)$$

Assuming that the chiral coupling constant κ is positive, the energy functional (2.32) has a global minimum for the phase $\delta = \pi/2$. It means that the magnetic Skyrmion possesses

an intrinsic internal orientation. The energy functional (2.32) for the profile function $\vartheta(r)$ in the topological sector $Q = -1$, with the minimal-energy orientation $\delta = \pi/2$, reduces to

$$E = 2\pi \int r dr \left(\frac{1}{2}(\vartheta')^2 + \frac{\sin^2 \vartheta}{2r^2} + \kappa \left(\vartheta' + \frac{\sin(2\vartheta)}{2r} \right) + h(1 - \cos \vartheta)^p \right). \quad (2.35)$$

The associated variational equation is

$$\vartheta'' + \frac{1}{r}\vartheta' + \frac{2\kappa}{r}\sin^2 \vartheta - \frac{1}{2r^2}\sin(2\vartheta) - hp \sin \vartheta (1 - \cos \vartheta)^{p-1} = 0. \quad (2.36)$$

Remarkably, for the possible existence of these solutions, a negative contribution to the energy of the DM interaction is a necessity. Many analytical works studied mathematical properties proving the theoretical existence of these stable solutions in chiral magnets [16, 18–21, 23, 51]. If we had chosen the boundary conditions for ϑ corresponding to those of an anti-Skyrmion: $\vartheta(0) = -\pi$ and $\vartheta(\infty) = 0$, the kinetic energy and potential energy would remain invariant, but the DM contribution to the energy would flip sign, making the anti-Skyrmion unstable. We thus understand that the chirality of the DM term selects either the Skyrmion or the anti-Skyrmion according to the sign of $\kappa \sin \delta$.

It will prove useful to consider the asymptotic behavior of the field ϑ found by linearizing (2.36). In particular, we find

$$\begin{cases} \vartheta = CK_1(\sqrt{hr}), & p = 1, \\ \vartheta = \frac{C}{r}, & p > 1, \end{cases} \quad (2.37)$$

where C is an undetermined constant and K_1 is the modified Bessel function of the second kind, that tends to zero exponentially. Notice that for the cases with $p > 1$, the profile function ϑ tends to its vacuum value with a power law and hence much slower than the cases with a Zeeman term.

At this point, we can analyze the symmetry group of the theory in the background of the soliton. The group of translations in the plane T_2 of Eq. (2.35) is broken by the soliton (2.31) and this symmetry breaking is responsible for two moduli defining the position of the magnetic Skyrmion. On the other hand, the rotational contribution is more complicated. If we consider the Lagrangian density in the vacuum without the DM term, the solitonic background, as we can verify looking at Eq. (2.31), breaks the $\text{SO}(2)_{\text{spt}} \times \text{SO}(2)_{\text{int}}$ group to $\text{SO}(2)_{\text{anti-diag}}$ (anti-diagonal). It means that the unbroken group is $\text{SO}(2)$ whose internal angle would be responsible for another modulus, i.e. the orientation δ of the Skyrmion. However, the soliton exhibits a similar symmetry-breaking effect as well in the DM interaction. Therefore, by considering both the background of the soliton and the DM interaction together, we observe that further symmetry breaking occurs for the two separate $\text{SO}(2)_{\text{diag}}$ groups, resulting in the fixing of the orientation angle δ . As we have previously discussed,

the energy is minimized when $\delta = \pi/2$. Fig. 1 shows a scheme of the symmetry-breaking effect responsible of fixing the δ -phase.

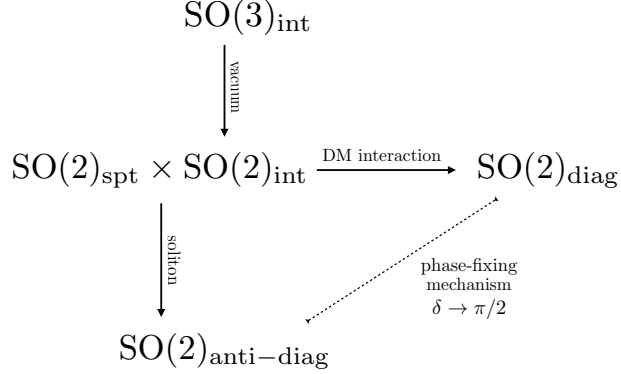


Figure 1: Schematic of the symmetry breaking mechanism for the compact symmetry group of the theory.

Finally, the moduli space \mathcal{M}_1 of a 2-dimensional magnetic Skyrmion has real dimension

$$\dim_{\mathbb{R}}(\mathcal{M}_1) = 2 , \quad (2.38)$$

due only to the translational zeromodes.

2.2 The DM term and integration-by-parts

It is well known that adding a total derivative to the energy does not change the equations of motion, but it may change the energy. The DM term in the canonical formulation with the hedgehog Ansatz (2.31) (with $Q = -1$) is written as

$$E_1 = 2\pi\kappa \int r dr \left(\vartheta' + \frac{\sin 2\vartheta}{2r} \right), \quad (2.39)$$

but integration by parts as in Eq. (2.16) yields

$$E_1^b = 4\pi\kappa \int r dr \sin^2(\vartheta)\vartheta' + \pi\kappa[r \sin 2\vartheta]_0^\infty, \quad (2.40)$$

where the latter is a total derivative. A different integration by parts can be performed, so as to eliminate ϑ' ,

$$E_1^c = 2\pi\kappa \int r dr \left(-\frac{\vartheta}{r} + \frac{\sin 2\vartheta}{2r} \right) + 2\pi\kappa[r\vartheta]_0^\infty. \quad (2.41)$$

If $p = 1$ the total derivatives simply vanish and they can safely be dropped without changing the energies. However, for the $p > 1$ cases, all three DM terms without the boundary terms

give rise to the same equation of motion, but different energies if the boundary terms are dropped.

We will see shortly, that we need to drop a boundary term and compute the DM energy with a modified term in order to predict the correct properties of the physical solution in the O(3) sigma model limit, which we shall study next.

2.3 O(3) sigma model limit

If we keep $\ell \equiv \kappa/h$ fixed and send $\epsilon \equiv \kappa^2/h \rightarrow 0$ we obtain the equation for the sigma model lump with just the E_2 contribution, which has the equation of motion

$$\vartheta'' + \frac{1}{r}\vartheta' - \frac{1}{2r^2}\sin(2\vartheta) = 0 . \quad (2.42)$$

The solution is

$$\vartheta(r) = 2 \arctan \frac{a}{r} , \quad (2.43)$$

with a an arbitrary scale of the soliton (size modulus of the O(3) sigma model lump). We then evaluate the energy functional for small but finite values of ϵ . It turns out that the energy functional (2.35) on this solution (2.43) as a function of a , by minimization with respect to a , gives rise to an incorrect result. Since we are considering a lump, the falloff of the profile function ϑ is power-like (see Eq. (2.37)) making the boundary terms in Eqs. (2.40) and (2.41) nonvanishing. It is thus necessary to consider the *right* energy functional, the one that gives the correct variational problem. The correct choice is either (2.40) or (2.41) without boundary terms. Evaluation of the full energy functional, without the boundary term of the DM, on the lump solution gives

$$E(a) = 4\pi - 8\pi\kappa a + \frac{2^p}{p-1}h\pi a^2 , \quad (2.44)$$

and in turn the lump size

$$a = \frac{p-1}{2^{p-2}}\ell . \quad (2.45)$$

Inserting the lump size back into the energy (2.44), we find

$$E = 4\pi - 4\pi\frac{(p-1)}{2^{p-2}}\epsilon . \quad (2.46)$$

We notice that the correction to the energy is linearly proportional to ϵ . This estimate, for $p = 2$, predicts that the Skyrmion phase is the stable phase (compared with the homogeneous ground state) when $\epsilon > 1$.² For the $p = \frac{3}{2}$ case, the corresponding critical

²We thank Bruno Barton-Singer for pointing this out to us.

coupling is $\epsilon^{\text{crit}} = \sqrt{2}$ in the lump approximation (in this case, the solution is not of lump type for ϵ large).

For $p = 1$ the solution for the lump (2.43) evaluated on E_0 diverges, see Eq. (2.44). Introducing a cutoff gives

$$E(a) \simeq 4\pi - 8\pi\kappa a + 2\pi a^2 h \log\left(1 + \frac{\Lambda^2}{a^2}\right). \quad (2.47)$$

Assuming that $\Lambda \gg a$, we can approximate $\log(1 + \Lambda^2/a^2) \simeq 2\log(\Lambda/a)$. Hence extremization with respect to a yields

$$a = -\frac{\ell}{\omega\left(-\frac{\sqrt{e}\ell}{\Lambda}\right)}, \quad (2.48)$$

where ω is the Lambert-W function, i.e. the inverse of the function $f(W) = We^W$, and $\sqrt{e} \simeq 1.649$. Expanding a in small $\ell = \kappa/h$ yields

$$a \simeq \frac{\Lambda}{\sqrt{e}} - \ell + \mathcal{O}(\ell^2\Lambda^{-1}). \quad (2.49)$$

Regularization of the infinity amounts to removing the term Λ , for which

$$a \simeq -\ell. \quad (2.50)$$

Unfortunately, this yields a negative lump size which is not physically viable.

Alternatively, we can consider extracting the “effective” lump size from the $\epsilon \rightarrow 0$ limit, numerically, and regularizing the energy yielding

$$E_{\text{reg}}(a) \simeq 4\pi - 4\pi c\epsilon, \quad (2.51)$$

with $a = c\ell$. The above considerations suggest that the lump size a goes to zero in the $\epsilon \rightarrow 0$ limit, probably logarithmically or with a slow power law.

2.4 Restricted model limit

In the case of ℓ fixed and $\epsilon \rightarrow \infty$ we expect that the stable Skyrmion is essentially given by a stabilization between E_1 and E_0 , while E_2 is negligible with respect to the other two terms. Thus the energy functional takes the simplified form³

$$E[\mathbf{n}] = \int d^2x \left(\kappa\epsilon_{iab}\partial^i n^a n^b + V_p(\mathbf{n}) + \frac{\lambda}{2}(\mathbf{n} \cdot \mathbf{n} - 1) \right). \quad (2.52)$$

³One may wonder why we restrict the potential to the form V_p of Eq. (2.5) and hence do not consider e.g. $V \propto (1 - (n^3)^2)$. Although such easy-axis potential is often utilized in magnetic systems, they do not allow for the large- ϵ limit because the ground state becomes inhomogeneous [52, 53] and requires a different analysis than carried out here.

We may call this model the “restricted” magnetic Skyrme model. The equations of motion are

$$hpN^a(1 - \mathbf{n} \cdot \mathbf{N})^{p-1} - 2\kappa\epsilon_{aib}\partial^i n^b - \lambda n^a = 0 , \quad (2.53)$$

where the Lagrange multiplier is

$$\lambda = n^a (hpN^a(1 - \mathbf{n} \cdot \mathbf{N})^{p-1} - 2\kappa\epsilon_{aib}\partial_i n_b) . \quad (2.54)$$

One interesting aspect of these equations is that they are first order in the derivative. Thus, they can easily be solved analytically. Unlike the restricted baby-Skyrme model [42–45], here we do not have an infinite dimensional symmetry group. The restricted equation for the hedgehog Ansatz has no derivatives and can be written as

$$\frac{\kappa}{r} \sin^2 \vartheta - \frac{hp}{2} \sin \vartheta (1 - \cos \vartheta)^{p-1} = 0 . \quad (2.55)$$

Solving for r as a function of ϑ , we obtain

$$r = \frac{2\ell \sin \vartheta}{p(1 - \cos \vartheta)^{p-1}} , \quad (2.56)$$

where $\ell = \frac{\kappa}{h}$. Some examples are:

$$p = 1 : \quad \vartheta(r) = \pi - \arcsin \rho(r) , \quad \rho(r) = \frac{r}{2\ell} , \quad (2.57)$$

$$p = \frac{3}{2} : \quad \vartheta(r) = 2 \arccos \rho(r) , \quad \rho(r) = \frac{3\sqrt{2}r}{8\ell} , \quad (2.58)$$

$$p = 2 : \quad \vartheta(r) = 2 \arctan \frac{1}{\rho(r)} , \quad \rho(r) = \frac{r}{\ell} , \quad (2.59)$$

with $\rho = \rho(r) \in [0, 1)$.

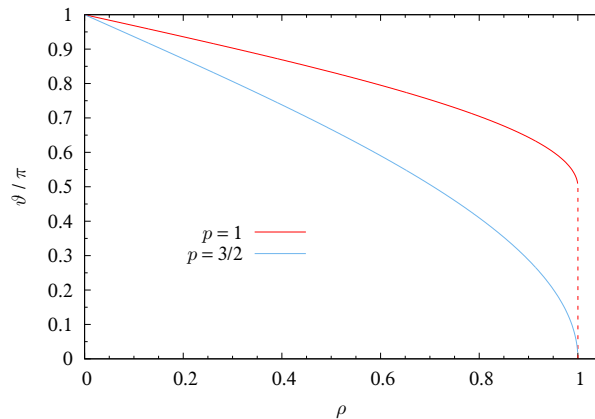


Figure 2: Compacton (blue) for $p = 3/2$ (2.58) supercompacton (red) for $p = 1$ (2.57). Notice that $\rho(r)$ has a different numerical prefactor of r/ℓ in each case.

For $p = 1$, an interesting new feature is present in the theory, a compact and discontinuous solution that we may call a *supercompacton*. As shown in Fig. 2, it differs from the usual compacton of the baby-Skyrme model by possessing a discontinuity. For $p < \frac{3}{2}$, the solution is discontinuous and covers only half of the sphere. For $p = \frac{3}{2}$ it is a compacton. For $p > \frac{3}{2}$, $\vartheta(r)$ goes to 0 smoothly as $r \rightarrow \infty$.

For a generic potential the condition for having a supercompacton is not necessarily related to the behavior close to the minimum of the potential. Let us consider, as potential, a generic function $V(\vartheta)$ with minimum at $\vartheta = 0$ whose expansion near the vacuum is given by $V(\vartheta) = \vartheta^{2p} + \dots$. The solution of the restricted model, in implicit form, is

$$r(\vartheta) = \frac{2\kappa \sin^2 \vartheta}{V'(\vartheta)} . \quad (2.60)$$

A supercompacton is defined as having a discontinuity in the profile function $\vartheta(r)$. This condition is met when the function $r(\vartheta)$ reaches a maximum at $\vartheta > 0$. Consequently, it is not necessarily related to the power-law near the vacuum. In the event that the function $r(\vartheta)$ is monotonic and attains a (finite) maximum at $\vartheta = 0$, the restricted solution is not a supercompacton.

2.5 Critical coupling

The critical coupling for the case of $p = 2$ can readily be seen from a Bogomol'nyi completion [19]

$$\begin{aligned} E &= 2\pi \int r \, dr \left[\frac{1}{2}(\vartheta')^2 + \frac{\sin^2 \vartheta}{2r^2} + \kappa \left(\vartheta' + \frac{\sin(2\vartheta)}{2r} \right) + h(1 - \cos \vartheta)^2 \right] \\ &= 2\pi \int r \, dr \left[\frac{1}{2} \left(\vartheta' - \frac{\sin \vartheta}{r} + \kappa(1 - \cos \vartheta) \right)^2 + \frac{\sin \vartheta}{r} \vartheta' + \frac{\kappa}{r} \partial_r (r \sin \vartheta) \right] \\ &= \pi \int r \, dr \left(\vartheta' - \frac{\sin \vartheta}{r} + \kappa(1 - \cos \vartheta) \right)^2 + 4\pi Q + 4\pi \Omega , \end{aligned} \quad (2.61)$$

which holds for $h = \frac{\kappa^2}{2}$ and

$$Q = \frac{1}{2} \int dr \sin(\vartheta) \vartheta' = -1 , \quad (2.62)$$

$$\Omega = \frac{\kappa}{2} \int dr \partial_r (r \sin \vartheta) = 2 , \quad (2.63)$$

which are the topological charge and a boundary term, respectively, where $\vartheta(0) = \pi$ and $\vartheta(\infty) = 0$. The Bogomol'nyi completion can also be understood as the BPS limit of

the gauged $\mathbb{C}P^1$ model with a particular choice of constant gauge field $A_i^a = -\kappa\delta_i^a$, that generates the DM term [19]. The energy (2.61) shows the Bogomol'nyi or BPS equation

$$\vartheta' - \frac{\sin \vartheta}{r} + \kappa(1 - \cos \vartheta) = 0 , \quad (2.64)$$

as well as the topological energy bound

$$E \geq 4\pi(Q + \Omega) = 4\pi , \quad (2.65)$$

with equality that holds only when the BPS equation is satisfied. The BPS equation is solved by

$$\vartheta = 2 \arctan \left(\frac{2}{\kappa r} \right) . \quad (2.66)$$

This is the $O(3)$ sigma model lump solution with lump size $a = \frac{2}{\kappa}$. We also notice that the BPS bound on the energy is 4π , just like the lump energy. Finally, we have used the asymptotic behavior of the solution $\vartheta \sim \frac{4}{\kappa r}$ at $r \rightarrow \infty$ in evaluating the boundary term Ω in Eq. (2.63).

We now consider what happens if we again drop the boundary term of Eq. (2.16) as we had to in the lump case of Sec. 2.3. The energy is thus changed by a total derivative, yielding now

$$\begin{aligned} E &= 2\pi \int r \, dr \left[\frac{1}{2} \left(\vartheta' - \frac{\sin \vartheta}{r} + \kappa(1 - \cos \vartheta) \right)^2 + \frac{\sin \vartheta}{r} \vartheta' + \frac{\kappa}{r} \partial_r (r \sin \vartheta (1 - \cos \vartheta)) \right] \\ &= \pi \int r \, dr \left(\vartheta' - \frac{\sin \vartheta}{r} + \kappa(1 - \cos \vartheta) \right)^2 + 4\pi Q + 4\pi \Omega' . \end{aligned} \quad (2.67)$$

Notice that a total derivative other than the topological charge remains

$$\Omega' = \frac{\kappa}{2} \int dr \, \partial_r (r \sin \vartheta (1 - \cos \vartheta)) = 0 . \quad (2.68)$$

which however vanishes when evaluated on the BPS solution. This means that dropping the boundary term in Eq. (2.16) leads to a Bogomol'nyi energy (bound)

$$E \geq -4\pi . \quad (2.69)$$

2.6 Analytic solution at any coupling

We note that the Bogomol'nyi completion requires us to select the critical coupling $h = \frac{\kappa^2}{2}$ enabling us to complete the square in the energy functional. This choice of coupling corresponds to $\epsilon = 2$. However, another interesting fact about the Zeeman squared potential

($p = 2$) is that inserting the Ansatz $\vartheta = 2 \arctan \frac{a}{r}$ into the full second-order Euler-Lagrange equation gives [19]

$$\frac{8a^2r(\kappa - ah)}{(a^2 + r^2)^2} = 0, \quad (2.70)$$

which beautifully has the solution $a = \frac{\kappa}{h} = \ell$. This size does not contradict the BPS solution, since the first-order BPS equation required $h = \frac{\kappa^2}{2}$ which in the full second-order solution corresponds to the lump size $a = \frac{\kappa}{h} = \frac{2}{\kappa}$. It is interesting, however to insert the exact solution into the energy functional (2.35), which gives

$$E = 2\pi \int r \, dr \frac{4h^2\kappa^2}{(h^2r^2 + \kappa^2)^2} = 4\pi. \quad (2.71)$$

But this is nothing but the lump energy. We see that the $p = 2$ case is a rather special case, where the energy is always the lump energy and the solution is always the lump solution with the lump size $a = \ell = \frac{\kappa}{h}$. However, only at the critical coupling, the second-order equation of motion reduces to the first-order BPS equation (2.64).⁴

The $p = 2$ case is thus applicable to many more physical systems, than just the critically coupled one [19]. Having the analytic solution in hand may be advantageous for further studies, including interaction and scattering etc.

In Sec. (2.3), we found however that the lump-type Ansatz gave the incorrect lump size a by using the energy (2.35), and we should instead drop the boundary term of Eq. (2.40) yielding the energy

$$E = 2\pi \int r \, dr \frac{4h\kappa^2(h^3r^2 + h(1 - 3hr^2)\kappa^2 + \kappa^4)}{(h^2r^2 + \kappa^2)^3} = 4\pi(1 - \epsilon). \quad (2.72)$$

We may interpret the change of sign of the energy at $\epsilon = \epsilon^{\text{crit}} = 1$ as the Skyrmionic phase being energetically preferable for $\epsilon > 1$ and the homogeneous phase on the other hand preferable for $\epsilon < 1$. Luckily, the BPS-case resides in the Skyrmionic phase at $\epsilon = 2$.

Since the $p = 2$ case is an exact solution for all values of ϵ , there is no need to perform numerical computations for this case.

2.7 Numerical solutions

For the general theory, we can solve equation (2.36) using a standard shooting method, beginning from the origin with the initial condition $\vartheta(0) = \pi$. The form of the solution close to the origin is $\vartheta(r) \simeq \pi - \alpha r$. By varying the angular coefficient c , we find only one solution in the topological sector $Q = -1$ as already shown in the literature [16, 18–21, 23, 51].

⁴The fact that this analytic solution holds for all values of the coupling, is somewhat similar to the situation in the baby-Skyrme model for $p = 4$ [42, 54].

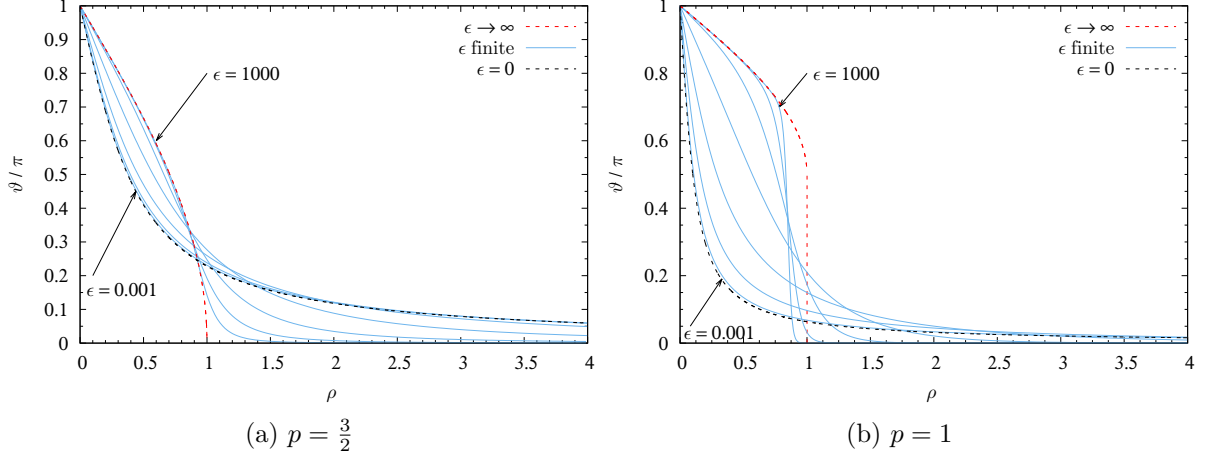


Figure 3: Profile function $\vartheta(\rho)$ for (a) $p = \frac{3}{2}$ and (b) $p = 1$ with $\epsilon = 0.001, 0.01, 0.1, 1, 10, 100, 1000$. The red-dashed curve corresponds to the restricted limit, whereas the black-dashed curve is the sigma-model lump limit with lump sizes (a) $a = \frac{\ell}{\sqrt{2}}$ and (b) $a = \ell/5$. The latter is chosen for illustrative purposes.

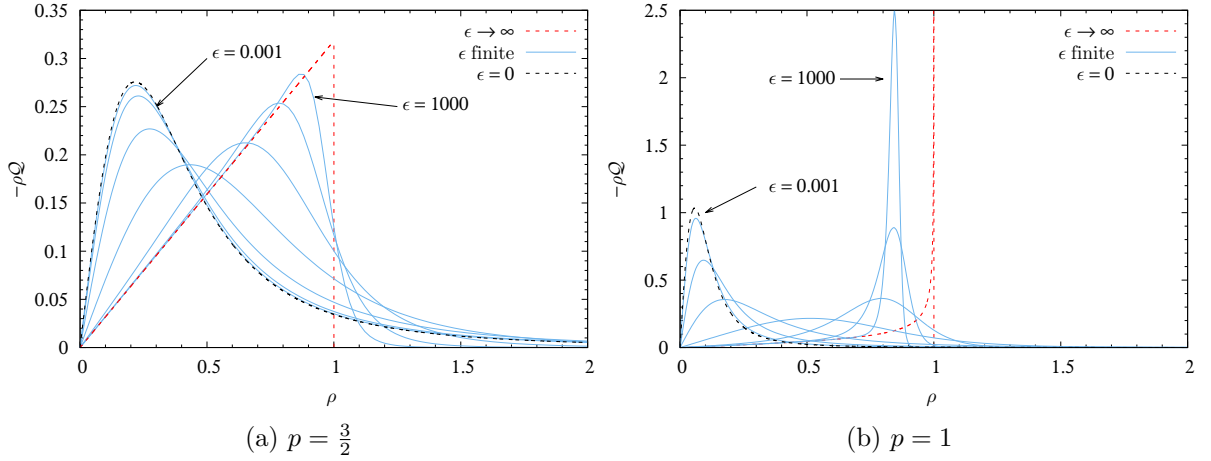


Figure 4: Topological charge density, \mathcal{Q} for (a) $p = \frac{3}{2}$ and (b) $p = 1$ with $\epsilon = 0.001, 0.01, 0.1, 1, 10, 100, 1000$. The topological charge densities of the lumps and restricted Skyrminion are shown with dashed black and red curves, respectively. In the $p = 1$ case, the size of the lump is selected for illustrative purpose, corresponding to the solutions in Fig. 3.

Let us now study how the theory behaves by varying the control parameters, ℓ and ϵ . We plot the solutions ϑ for a variety of couplings, ϵ , for $p = \frac{3}{2}$ (panel (a)) and $p = 1$ (panel (b)) in Fig. 3. In each case, we plot ϑ as a function of ρ which is proportional to r/ℓ , such that ℓ -dependence is removed from the solutions and ρ is defined in Eqs. (2.57)-(2.58). We see that as ϵ goes from 0 to ∞ the solution flows from the sigma model lump solutions (black dashed lines) to the restricted (compacton) solution (red dashed lines) in both cases. In the $p = \frac{3}{2}$ case, the lump solution (2.43) with a lump size (2.45) is shown and the restricted solution is that of Eq. (2.58). We notice that the numerical solutions tend to the lump solution with the correct lump size (2.45), where a boundary term has been discarded when determining the lump size from the energy functional. In the $p = 1$ case, on the other hand, we have set the lump size to $a = \frac{\ell}{5}$ by hand for visualization purposes and the restricted supercompacton solution that the solutions flow to for large ϵ is given in Eq. (2.57). We see again that the lump solution matches well with the numerical solutions, but the lump size is set by hand for comparison with the solution at small $\epsilon = 10^{-3}$. We will shortly argue that the lump size should go to zero in the limit $\epsilon \rightarrow 0$. Note that the supercompacton has a discontinuity and covers only half of the 2-sphere, from the south pole to the equator. At finite ϵ , the discontinuity is resolved and topological soliton covers the entire sphere. As $\epsilon \rightarrow \infty$, a step-function type discontinuity is created and the missing half of the sphere is mapped into a very narrow region.

Fig. 4 shows the topological charge density that integrates to $Q = -1$, in the $p = \frac{3}{2}$ case (panel (a)) and in the $p = 1$ case (panel (b)).

Fig. 5 shows the energy densities for the sigma-model lump limit ($\epsilon \rightarrow 0$) in panels (a) and (b) with and without the boundary term for $p = \frac{3}{2}$ and $p = 1$, respectively, and for the restricted limit ($\epsilon \rightarrow \infty$) in panels (c) and (d) for $p = \frac{3}{2}$ and $p = 1$, respectively, with the boundary term and in panels (e) and (f) $p = \frac{3}{2}$ and $p = 1$, respectively, without the boundary term of Eq. (2.40). In both the charge density as well as in the energy density, the discontinuity that develops in the $p = 1$ case for $\epsilon \rightarrow \infty$ is clearly seen in Figs. 4(b) and 5(d), respectively. We note that the energy density is divergent (singular) in the $p = \frac{3}{2}$ case at $\rho = 1$ when the boundary term is taken into account, see Fig. 5(c), but is convergent (finite) when the boundary term is dropped, see Fig. 5(e). We also note that the total energy (the integral) is unchanged in the $p = 1$ case (see Figs. 5(d) and 5(f)), but the energy density is slightly modified by the presence of the boundary term.

We show the total energy of the numerical solutions in the lump limit ($\epsilon \rightarrow 0$) for the $p = \frac{3}{2}, 1$ cases in Fig. 6(a). We notice that the $p = \frac{3}{2}$ case is well described by the energy functional (2.46) with the correct lump size (2.45). This confirms that discarding the boundary term in Eq. (2.40) is appropriate for computing the energies in the lump limit. In the $p = 1$ case, we show the regularized energy (2.47) with a dashed red curve and lump size a as chosen in Fig. 3. We show the sign change of the energy in the $p = \frac{3}{2}, 1$

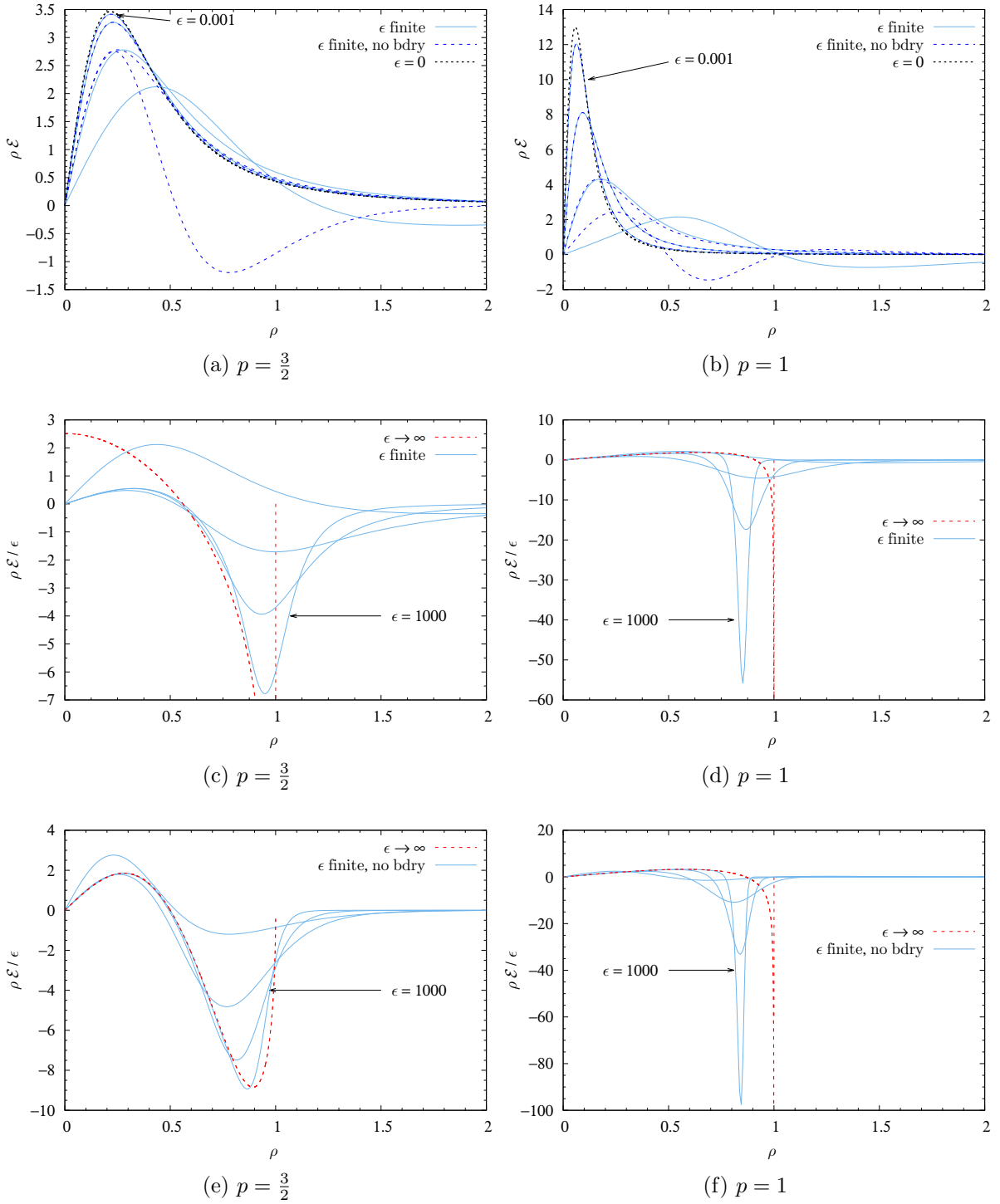


Figure 5: Energy density for: (a) $p = \frac{3}{2}$ (b) $p = 1$ and $\epsilon = 0.001, 0.01, 0.1, 1$ with the boundary term of Eq. (2.40) (solid blue lines) and without it (dashed dark-blue lines), and in (c) $p = \frac{3}{2}$ (d) $p = 1$ and $\epsilon = 1, 10, 100, 1000$ with the boundary term and in (e) $p = \frac{3}{2}$ (f) $p = 1$ and $\epsilon = 1, 10, 100, 1000$ without the boundary term of Eq. (2.40).

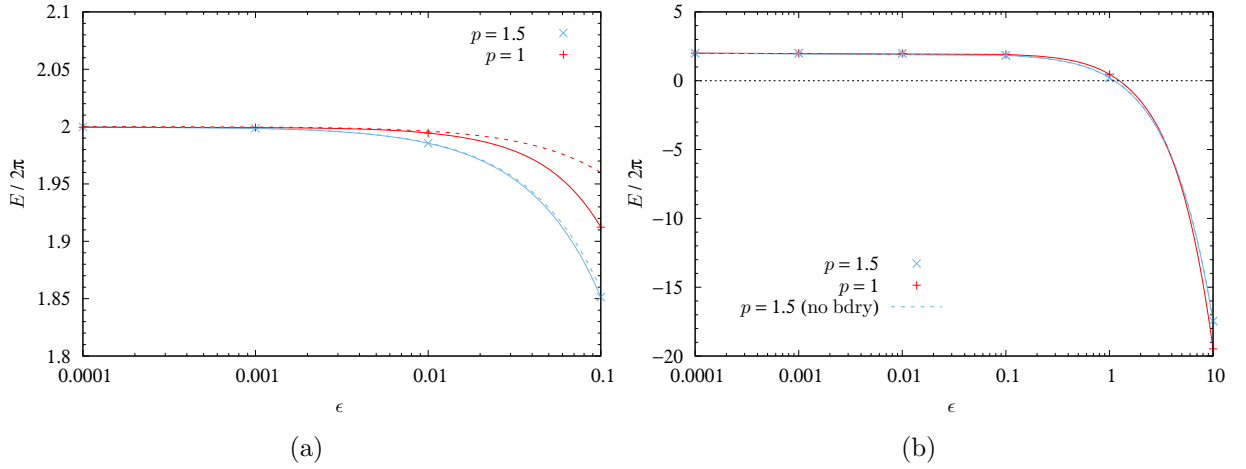


Figure 6: Energy in the lump limit ($\epsilon \rightarrow 0$) as a function of ϵ for $p = \frac{3}{2}$ and $p = 1$. (a) The blue dashed line corresponds to the analytical energy formula (2.46) for the lump in the limit of small but nonvanishing ϵ in the case of $p = \frac{3}{2}$. The red dashed line instead is the energy of Eq. (2.51) with the lump size taken from Fig. 3. (b) The energy shown up to larger values of ϵ revealing the sign change near $1 < \epsilon < 2$. The case $p = \frac{3}{2}$ is shown with (solid blue line) and without the boundary term (dashed blue line) of Eq. (2.40).

case in Fig. 6(b) which appears to take place around $1 < \epsilon < 2$, which is consistent with the lump prediction (2.46) which for $p = \frac{3}{2}$ should take place at $\epsilon = \epsilon^{\text{crit}} = \sqrt{2}$.

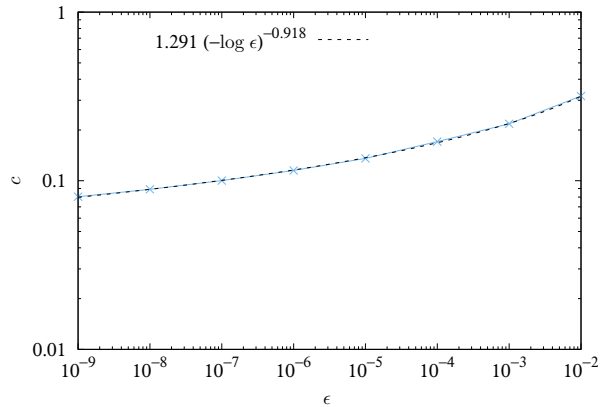


Figure 7: The lump size $c = \frac{a}{\ell}$ estimated by fitting the lump solution to the numerical solutions. The dashed black curve is a logarithmic fit.

Finally, we consider the difficult problem of estimating the lump size in the $\epsilon \rightarrow 0$ limit. Since we can see from Fig. 3 that the profiles match the lump solution if the lump size is fitted correctly, we can extract this lump size from the numerical solutions by fitting the

size of the lump solution to the numerical ones. Fig. 7 shows the numerically extracted lump sizes and a logarithmic fit finding an approximate behavior of the lump size as $c \approx 1.291(-\log \epsilon)^{-0.918}$. Clearly the lump size goes very slowly to zero.

2.8 Comparison with experiments

We have confirmed that the magnetic Skyrmion model, up to rescaling of energy and length, is essentially a one-parameter model (2.24)-(2.25). This parameter, ϵ , controls the relation between E_2 and $E_1 + E_0$. In both the large- ϵ and the small- ϵ limit, analytic approximations are available, see Secs. 2.3 and 2.4. It may be interesting to explore various phenomenological realizations of chiral magnets and determine the order of magnitude of the parameter ϵ that can be realized.

The typical Skyrmion size, determined by the DM interaction, in chiral magnets, e.g. MnSi [28, 33], is about $\ell \simeq 5 - 100$ nm. From the phase diagram for MnSi [26], the range for the external magnetic field in the Skyrmion phase is $B \sim 0.1 - 0.3$ T. Another important experimental parameter is λ , the period of the spiral, determined by the ratio of the dipolar and exchange interactions:

$$\lambda = \frac{2\pi J}{D} . \quad (2.73)$$

Such parameter is well known for different chiral magnets (see e.g. Table 1 in Ref. [33]), in the case of MnSi: $\lambda = 18$ nm. From Eq. (2.22), we get

$$\begin{aligned} J &= \frac{\lambda D}{2\pi} = \frac{\lambda \ell |B|}{4\pi} , \\ \epsilon &= \frac{4D^2}{J|B|} = 4\pi \frac{\ell}{\lambda} . \end{aligned} \quad (2.74)$$

Using the minimal values for the previous parameters (for MnSi) defined on a range of values, i.e. $B \sim 10^{-1}$ T, $\ell \sim 10$ nm, and $\lambda \simeq 10$ nm, we find

$$\begin{aligned} J &\simeq 100 \text{ nm}^2 \times \text{T} \simeq 10^{-14} \text{ J} , \\ \epsilon &\simeq 10 , \end{aligned} \quad (2.75)$$

where J is the unit *Joule*, not to be confused with the interaction strength of the Heisenberg Hamiltonian. Note that in general ℓ can change significantly, viz. one order of magnitude. For instance, if we fix $\ell = 100$ nm and $\lambda \in \mathcal{O}(10^1)$ nm as before, we find that ϵ changes one order of magnitude, i.e. $\epsilon \simeq 100$. For materials other than MnSi, e.g. $\text{Fe}_{1-x}\text{Co}_x\text{Si}$ or $\text{Mn}_{1-x}\text{Fe}_x\text{Ge}$, λ can also be of the order $\mathcal{O}(10^2)$ nm. Therefore, considering the other two cases where λ is fixed as $\lambda \sim 10^2$ nm and ℓ takes its maximum and minimum values, we

find the relevant ranges for ϵ :

$$\begin{aligned} 1 \lesssim \epsilon \lesssim 10, & \quad \ell \simeq 10 \text{ nm}, \\ 10 \lesssim \epsilon \lesssim 100, & \quad \ell \simeq 100 \text{ nm}. \end{aligned} \tag{2.76}$$

Finally, the approximating limits studied in this work can be seen to be relevant for describing certain experimental 2D magnetic Skyrmions within the ranges given in the above equation.

In Secs. 2.5 and 2.6, we saw that in the special physical case of $p = 2$, which describes chiral magnets with anisotropy interactions, any spherical magnetic Skyrmion can be represented by the analytical lump solution, regardless of its DM coupling, κ . However, the potential $V_{p=2}$ corresponds to the sum of a magnetic field and anisotropy (easy-plane) contributions. To realize this potential, the couplings of the anisotropy term must be exactly half of that of the Zeeman term. It turns out to be possible [55]. Furthermore, since the critical coupling regime corresponds to the condition $\forall \ell, \epsilon = 2$, which satisfies the inequalities (2.76), we suggest that, in principle, a BPS magnetic Skyrmion could be realized experimentally.

3 Conclusion

In this paper, we have studied magnetic Skyrmions in chiral magnets with three different potentials, corresponding to $p = 1$, $p = \frac{3}{2}$ and $p = 2$ in the limits of the control parameter $\epsilon = \frac{\kappa^2}{h} = \frac{4D^2}{|B|J}$ becoming very large and going to zero. The $p = 1$ case is simply the Zeeman potential term and the $p = 2$ case is a particular combination of the easy-plane (anisotropy) and the Zeeman potentials. The $p = \frac{3}{2}$ case is probably somewhat more academic. The ϵ vanishing limit reduces the Skyrmion to a sigma model lump with a lump size that we accurately estimated, except for the case of the Zeeman term ($p = 1$). The large- ϵ limit instead corresponds to the “restricted” magnetic Skyrmions, for which we found the exact analytic solutions as well. In the $p = \frac{3}{2}$ case, the restricted solution is a compacton, similar in nature to those found in the baby-Skyrme [43–45] and 3D Skyrme models [46]. However, in the $p = 1$ case corresponding to the Zeeman term, we find a *new* type of restricted solution, which we dub a *supercompacton*, since it becomes discontinuous. We provide numerical solutions showing that they slowly tend to the supercompacton limit for very large values of ϵ . We have also reviewed the beautiful result of the critically coupled magnetic Skyrmion of Barton-Singer-Ross-Schroers [19], where an analytic solution is available, hence providing many studies with a clear advantage. Their solution is known to be an exact solution for any value of the coupling ϵ [19], but we find here that dropping the boundary term that leads to the correct lump size for this solution also changes the energy from the lump energy for all values of ℓ to the energy functional $4\pi(1 - \epsilon)$. This

energy functional changes sign at $\epsilon = 1$ suggesting $\epsilon = 1$ being the critical coupling for having the Skyrmionic phase.

Future directions that would be interesting to study, would be to utilize the exact analytic solutions for dynamical problems such as acceleration, interaction and scattering. Extending the planar materials to 3D materials may also be interesting, where numerical computations have found braiding magnetic Skyrmion solutions [56]. Using various limits, perhaps analytic insight can be found also in such cases.

Acknowledgments

We thank Bruno Barton-Singer for comments on our draft. The work of S. B. is supported by the INFN special research project grant ‘‘GAST’’ (Gauge and String Theories). S. B. G. thanks the Outstanding Talent Program of Henan University and the Ministry of Education of Henan Province for partial support. The work of S. B. G. is supported by the National Natural Science Foundation of China (Grant No. 12071111) and by the Ministry of Science and Technology of China (Grant No. G2022026021L). R. M. thanks the Department of Physics ‘‘E. Fermi’’ of University of Pisa where this work was initiated.

A Continuum Limit

The Heisenberg term of the GL energy density can be derived from the continuum limit of the lattice Hamiltonian

$$\mathcal{H}_H = -J \sum_{i,\mu} \mathbf{n}_i \cdot \mathbf{n}_{i+a\hat{e}_\mu}, \quad (\text{A.1})$$

where $a\hat{e}_\mu$ is the vector connecting the i -lattice site with its neighboring sites $i + a\hat{e}_\mu$, on a square ($\mu = x, y$) lattice. Assuming a small lattice constant a , one can perform a Taylor expansion on $\mathbf{n}_{i+a\hat{e}_\mu}$, i.e.,

$$\mathbf{n}_{i+a\hat{e}_\mu} \simeq \mathbf{n}_i + a\partial_\mu \mathbf{n}_i + (a^2/2)\partial_\mu^2 \mathbf{n}_i + \dots \quad (\text{A.2})$$

and insert it into Eq. (A.1). One finds that first term $\mathbf{n}_i \cdot \mathbf{n}_i$ is equal to the unity and can be discarded as a constant term. The second term, proportional to $\mathbf{n}_i \cdot \partial_\mu \mathbf{n}_i$, vanishes due to nonlinear constraint $\mathbf{n} \cdot \mathbf{n} = 1$. However, the third term

$$\mathcal{H}_H \approx -\frac{1}{2}Ja^2 \sum_i \mathbf{n}_i \cdot \partial_\mu^2 \mathbf{n}_i, \quad (\text{A.3})$$

in the continuum limit, $a \rightarrow 0$, and after an integration by parts, leads to a non-vanishing contribution, i.e.,

$$E_2[\mathbf{n}] = \frac{1}{2}J \int d^2x (\partial_\mu \mathbf{n} \cdot \partial_\mu \mathbf{n}), \quad \mathbf{n} \cdot \mathbf{n} = 1. \quad (\text{A.4})$$

The DM interaction, at the lattice level can be written as

$$\mathcal{H}_{\text{DM}} = -D \sum_{i,\mu} \hat{\mathbf{e}}_{\mu} \cdot (\mathbf{n}_i \times \mathbf{n}_{i+a\hat{\mathbf{e}}_{\mu}}) , \quad (\text{A.5})$$

where we expressed the DM vector as $\mathbf{D} = D\hat{\mathbf{e}}_{\mu}$. Upon Taylor expansion, the first derivative of $\mathbf{n}_{i+a\hat{\mathbf{e}}_{\mu}}$, provides the non-null contribution

$$\mathcal{H}_{\text{DM}} \approx Da \sum_{i,\mu} \mathbf{n}_i \cdot (\hat{\mathbf{e}}_{\mu} \times \partial_{\mu} \mathbf{n}_i) = Da \sum_i \mathbf{n}_i \cdot (\nabla \times \mathbf{n}_i) , \quad (\text{A.6})$$

where at the second step we have applied the vector definition for the curl operator. Thus, in the continuum limit, one finds

$$E_1[\mathbf{n}] = Da^{-1} \int d^2x \mathbf{n} \cdot (\nabla \times \mathbf{n}) , \quad (\text{A.7})$$

which corresponds to the usual DM energy functional. Finally, let us consider the potential-like term $-\mathbf{B} \cdot \mathbf{n}$ that describes the Zeeman interaction with an external magnetic field, which we choose to be aligned along the third direction, $\mathbf{B} = B\mathbf{e}_3$. Since we have arbitrarily chosen the vacuum field $\mathbf{N} = \mathbf{e}_3$, and we need the potential to vanish when evaluated on the vacuum, the energy contribution can be written as $E_0[\mathbf{n}] = B(1 - \mathbf{N} \cdot \mathbf{n}) = B(1 - n_3)$. Such potential contribution can be generalized to a class of potentials V_p of the form (2.5). At this point, by considering all the three contributions to the whole energy functional $E[\mathbf{n}]$ one gets Eq. (2.3).

References

- [1] R. Rajaraman, *Solitons and instantons*, Elsevier (1987) .
- [2] N. Manton and P. Sutcliffe, *Topological Solitons*, Cambridge Monographs on Mathematical Physics. Cambridge University Press, 2004, [10.1017/CBO9780511617034](https://doi.org/10.1017/CBO9780511617034).
- [3] H.-B. Braun, *Topological effects in nanomagnetism: from superparamagnetism to chiral quantum solitons*, *Advances in Physics* **61** (2012) 1.
- [4] M. Shifman, *Advanced Topics in Quantum Field Theory: A Lecture Course*. Cambridge University Press, 2012, [10.1017/CBO9781139013352](https://doi.org/10.1017/CBO9781139013352).
- [5] Y. M. Shnir, *Topological and Non-Topological Solitons in Scalar Field Theories*, Cambridge Monographs on Mathematical Physics. Cambridge University Press, 2018, [10.1017/9781108555623](https://doi.org/10.1017/9781108555623).
- [6] J. H. Han, *Skyrmions in condensed matter*, vol. 278. Springer, 2017, [10.1007/978-3-319-69246-3](https://doi.org/10.1007/978-3-319-69246-3).

- [7] T. H. R. Skyrme, *A non-linear field theory*, *Proceedings of the Royal Society of London. Series A. Mathematical and Physical Sciences* **260** (1961) 127.
- [8] T. H. R. Skyrme, *A unified field theory of mesons and baryons*, *Nuclear Physics* **31** (1962) 556.
- [9] A. Belavin and A. Polyakov, *Metastable states of two-dimensional isotropic ferromagnets*, *JETP letters* **22** (1975) 245.
- [10] A. N. Bogdanov and D. Yablonskii, *Thermodynamically stable “vortices” in magnetically ordered crystals. the mixed state of magnets*, *Zh. Eksp. Teor. Fiz* **95** (1989) 178.
- [11] A. Bogdanov and A. Hubert, *Thermodynamically stable magnetic vortex states in magnetic crystals*, *Journal of Magnetism and Magnetic Materials* **138** (1994) 255.
- [12] U. K. Rößler, A. N. Bogdanov and C. Pfleiderer, *Spontaneous skyrmion ground states in magnetic metals*, *Nature* **442** (2006) 797.
- [13] U. Rossler, A. A. Leonov and A. N. Bogdanov, *Chiral Skyrmionic matter in non-centrosymmetric magnets*, *J. Phys. Conf. Ser.* **303** (2011) 012105 [[1009.4849](#)].
- [14] M. Ezawa, *Compact Skyrmions, Merons and Bimerons in Thin Chiral Magnetic Films*, *Phys. Rev. B* **83** (2011) 100408 [[1010.4119](#)].
- [15] S. Banerjee, J. Rowland, O. Erten and M. Randeria, *Skyrmions in two-dimensional chiral magnets*, *Phys. Rev. X* **4** (2014) 031045 [[1402.7082](#)].
- [16] C. Melcher, *Chiral skyrmions in the plane*, *Proceedings of the Royal Society A: Mathematical, Physical and Engineering Sciences* **470** (2014) 20140394.
- [17] F. N. Rybakov and N. S. Kiselev, *Chiral magnetic skyrmions with arbitrary topological charge*, *Phys. Rev. B* **99** (2019) 064437 [[1806.00782](#)].
- [18] B. J. Schroers, *Gauged Sigma Models and Magnetic Skyrmions*, *SciPost Phys.* **7** (2019) 030 [[1905.06285](#)].
- [19] B. Barton-Singer, C. Ross and B. J. Schroers, *Magnetic Skyrmions at Critical Coupling*, *Commun. Math. Phys.* **375** (2020) 2259 [[1812.07268](#)].
- [20] V. M. Kuchkin, B. Barton-Singer, F. N. Rybakov, S. Blügel, B. J. Schroers and N. S. Kiselev, *Magnetic skyrmions, chiral kinks and holomorphic functions*, *Phys. Rev. B* **102** (2020) 144422 [[2007.06260](#)].
- [21] C. Ross, N. Sakai and M. Nitta, *Skyrmion interactions and lattices in chiral magnets: analytical results*, *JHEP* **02** (2021) 095 [[2003.07147](#)].

- [22] D. Hill, V. Slastikov and O. Tchernyshyov, *Chiral magnetism: a geometric perspective*, *SciPost Phys.* **10** (2021) 078.
- [23] B. Schroers, *Solvable Models of Magnetic Skyrmions*, in *11th International Symposium on Quantum Theory and Symmetries*, 10, 2019, [1910.13907](https://doi.org/10.13907), DOI.
- [24] Y. Amari, Y. Akagi, S. B. Gudnason, M. Nitta and Y. Shnir, *CP2 skyrmion crystals in an SU(3) magnet with a generalized Dzyaloshinskii-Moriya interaction*, *Phys. Rev. B* **106** (2022) L100406 [[2204.01476](https://arxiv.org/abs/2204.01476)].
- [25] F. Hanada and N. Sawado, *A baby Skyrme model with anisotropic DM interaction: Compact skyrmions revisited*, *Nucl. Phys. B* **996** (2023) 116377 [[2303.15751](https://arxiv.org/abs/2303.15751)].
- [26] A. Fert, V. Cros and J. Sampaio, *Skyrmions on the track*, *Nature Nanotechnology* **8** (2013) 152.
- [27] A. Fert, N. Reyren and V. Cros, *Magnetic skyrmions: advances in physics and potential applications*, *Nature Reviews Materials* **2** (2017) 17031.
- [28] S. Mühlbauer, B. Binz, F. Jonietz, C. Pfleiderer, A. Rosch, A. Neubauer et al., *Skyrmion Lattice in a Chiral Magnet*, *Science* **323** (2009) 1166767.
- [29] W. Münzer, A. Neubauer, T. Adams, S. Mühlbauer, C. Franz, F. Jonietz et al., *Skyrmion lattice in the doped semiconductor $fe_{1-x}co_xSi$* , *Phys. Rev. B* **81** (2010) 041203.
- [30] X. Z. Yu, Y. Onose, N. Kanazawa, J. H. Park, J. H. Han, Y. Matsui et al., *Real-space observation of a two-dimensional skyrmion crystal*, *Nature* **465** (2010) 901.
- [31] S. Seki, X. Z. Yu, S. Ishiwata and Y. Tokura, *Observation of skyrmions in a multiferroic material*, *Science* **336** (2012) 198.
- [32] X. Z. Yu, N. Kanazawa, Y. Onose, K. Kimoto, W. Z. Zhang, S. Ishiwata et al., *Near room-temperature formation of a skyrmion crystal in thin-films of the helimagnet fege*, *Nature Materials* **10** (2011) 106.
- [33] N. Nagaosa and Y. Tokura, *Topological properties and dynamics of magnetic skyrmions*, *Nature Nanotechnology* **8** (2013) 899.
- [34] Y. Tokura and N. Kanazawa, *Magnetic skyrmion materials*, *Chemical Reviews* **121** (2021) 2857.
- [35] K. Everschor-Sitte, J. Masell, R. M. Reeve and M. Kläui, *Perspective: Magnetic skyrmions—Overview of recent progress in an active research field*, *Journal of Applied Physics* **124** (2018) 240901.
- [36] S. Luo and L. You, *Skyrmion devices for memory and logic applications*, *APL Materials* **9** (2021) 050901.

- [37] C. Psaroudaki, E. Peraticos and C. Panagopoulos, *Skyrmion qubits: Challenges for future quantum computing applications*, *Applied Physics Letters* **123** (2023) 260501.
- [38] I. Dzyaloshinsky, *A thermodynamic theory of “weak” ferromagnetism of antiferromagnetics*, *Journal of Physics and Chemistry of Solids* **4** (1958) 241.
- [39] T. Moriya, *Anisotropic superexchange interaction and weak ferromagnetism*, *Phys. Rev.* **120** (1960) 91.
- [40] T. Moriya, *New mechanism of anisotropic superexchange interaction*, *Phys. Rev. Lett.* **4** (1960) 228.
- [41] P. Bak and M. H. Jensen, *Theory of helical magnetic structures and phase transitions in mnsi and fege*, *Journal of Physics C: Solid State Physics* **13** (1980) L881.
- [42] S. Bolognesi and W. Zakrzewski, *Baby Skyrme Model, Near-BPS Approximations and Supersymmetric Extensions*, *Phys. Rev. D* **91** (2015) 045034 [[1407.3140](#)].
- [43] T. Gisiger and M. B. Paranjape, *Solitons in a baby Skyrme model with invariance under volume / area preserving diffeomorphisms*, *Phys. Rev. D* **55** (1997) 7731 [[hep-ph/9606328](#)].
- [44] C. Adam, P. Klimas, J. Sanchez-Guillen and A. Wereszczynski, *Compact baby skyrmions*, *Phys. Rev. D* **80** (2009) 105013 [[0909.2505](#)].
- [45] C. Adam, T. Romanczukiewicz, J. Sanchez-Guillen and A. Wereszczynski, *Investigation of restricted baby Skyrme models*, *Phys. Rev. D* **81** (2010) 085007 [[1002.0851](#)].
- [46] C. Adam, J. Sanchez-Guillen and A. Wereszczynski, *A Skyrme-type proposal for baryonic matter*, *Phys. Lett. B* **691** (2010) 105 [[1001.4544](#)].
- [47] P. Klimas, L. C. Kubaski, N. Sawado and S. Yanai, *Gauged compact Q-balls and Q-shells in a multi-component CP^N model*, [2311.13076](#).
- [48] P. Klimas and L. R. Livramento, *Compact Q-balls and Q-shells in CPN type models*, *Phys. Rev. D* **96** (2017) 016001 [[1704.01132](#)].
- [49] C. Adam, P. Klimas, J. Sanchez-Guillen and A. Wereszczynski, *Compact gauge K vortices*, *J. Phys. A* **42** (2009) 135401 [[0811.4503](#)].
- [50] B. M. A. G. Piette, B. J. Schroers and W. J. Zakrzewski, *Multi - solitons in a two-dimensional Skyrme model*, *Z. Phys. C* **65** (1995) 165 [[hep-th/9406160](#)].
- [51] E. Walton, *On the geometry of magnetic Skyrmions on thin films*, *J. Geom. Phys.* **156** (2020) 103802 [[1908.08428](#)].
- [52] A. Bogdanov and A. Hubert, *Thermodynamically stable magnetic vortex states in magnetic crystals*, *Journal of Magnetism and Magnetic Materials* **138** (1994) 255.

- [53] S. Komineas and N. Papanicolaou, *Traveling skyrmions in chiral antiferromagnets*, *SciPost Phys.* **8** (2020) 086.
- [54] R. A. Leese, M. Peyrard and W. J. Zakrzewski, *Soliton Scatterings in Some Relativistic Models in (2+1)-dimensions*, *Nonlinearity* **3** (1990) 773.
- [55] S. Banerjee, J. Rowland, O. Erten and M. Randeria, *Enhanced stability of skyrmions in two-dimensional chiral magnets with rashba spin-orbit coupling*, *Phys. Rev. X* **4** (2014) 031045.
- [56] F. Zheng, F. N. Rybakov, N. S. Kiselev, D. Song, A. Kovács, H. Du et al., *Magnetic skyrmion braids*, *Nature Communications* **12** (2021) 5316.